1.3 REFRACTIVE TURBULENCE IN THE UPPER TROPOSHERE AND LOWER STRATOSPHERE: ANALYSIS OF AIRCRAFT MEASUREMENTS USING STRUCTURE FUNCTIONS

Donald Wroblewski *, Aerospace and Mechanical Engineering, Boston University,
Owen R. Cote, Air Force Research Laboratory (AFRL), Space Vehicle Directorate, Hanscom AFB,
Jorg M. Hacker, Airborne Research Australia, Flinders University,
Timothy L. Crawford, NOAA/ERL/ARL, Idaho Falls, and Ronald J. Dobosy, NOAA/ERL/ARL, Oak Ridge.

1. INTRODUCTION

.

For infrared and optical wavelengths, refractive turbulence is characterized mainly by the structure constant, $C_T^2 = D_{TT}(r)r^{-2/3}$, where $D_{TT}(r)$ is the structure function, defined as $D_{TT}(r) = <[T(r_0)-T(r_0+r)]^2>$. Two key assumptions are required: (1) the turbulence is locally isotropic within a range of length scales used to define the structure constant, so that the r may be defined in any direction, and (2) the turbulence obeys Kolmogorov scaling, i.e., the structure function follows an $r^{2/3}$ behavior characteristic of the inertial subrange. Traditionally, C_T^2 is not found through analysis of structure function, but indirectly through analysis of the corresponding spectra. For structure functions that obey an r^{γ} relation, where $0<\gamma<2$, the spectra will exhibit a corresponding $k^{-(1+\gamma)}$ relationship (Monin and Yaglom, 1975), where k is the wave number. Once a region is identified that exhibits a –5/3 slope on a log-log plot of the spectra, E_{θ}, versus k, C_T^2 is found from $C_T^2 = C_{\theta}/4$ where $C_{\theta} = E_{\theta}k^{5/3}$.

Analysis of the temperature structure function, D_{TT}, as opposed to spectra, can facilitate the determination of C_T^2 because the curves tend to be smoother, so that regions of constant slope are more easily identified. This paper will describe the use of structure functions, as opposed to spectra, for determining structure constants, as applied to turbulence data acquired during several aircraft data collection campaigns flown over the past four years. The basic approach will be discussed, and the advantage of this approach compared to spectra will be highlighted. In addition, the use of structure functions for short time intervals, including climb and descent flight segments, will also be presented. The implications of the results for the Airborne Laser Program and for future measurement campaigns will be discussed.

The data used for this work was acquired from the GROB 520T EGRETT, a high altitude research aircraft, equipped with three NOAA/FRD built BAT probes, featuring a nine-hole pressure probe for velocity measurements and a micro-bead thermistor for temperature (Crawford and Dobosy, 1992). Two of the probes were located on the wing, and one was located on the tail. The aircraft was flown approximately upwind or downwind, with level flight segments of constant altitude between 800 and 1,800 seconds, corresponding to approximately 60 to 150 km range.

The structure function for the temperature was found using r in the direction of flight relative to the wind: $D_{TT}(z,r) = <[T(z,t)-T(z,t+r/U_c)]^2>$ where $\tau = r/U_c$ is the lag time and U_c is the convection velocity of the flow past the probe (estimated as the mean true air speed of the aircraft at a given altitude, z). The smallest scale that can be resolved is between 1.4 and 2 m, based on the air speed and the sampling interval. From graphs of D_{TT} versus r, the inertial subrange was identified based on classic scaling laws, and power law curve fits were generated for estimating the structure constants. For temperature, $D_{TT}(r) = C_T^2 r^{2/3}$ and for velocities, $D_{UU}(r) = C_U^2 r^{2/3}$. Structure functions for the Reynolds heat fluxes were also analyzed.

The horizontal velocity was transformed from an aircraft coordinate frame into a coordinate system aligned with the mean wind direction, found from the mean horizontal velocities over the length of data record analyzed. In this coordinate system, the mean U velocity is the mean wind speed and the mean component of the V velocity is zero.

2. RESULTS: AUSTRALIA 8 AUG., 1999

Figure 1 shows a plot of D_{TT} versus separation distance, for data obtained at 9.65 km. during the 1999 Australia campaign, the strongest turbulence encountered during any of the campaigns. (Note that there are two separate segments at 9.65 km for this date—a low turbulence segment, designated 9.65A and the strong turbulence segment, designated 9.65B). The 2/3 slope characteristic of the inertial subrange is clearly identifiable for separation distances from about 25 m up to 200 m, providing for a good estimate of

Corresponding author address: Donald Wroblewski, Boston University, Dept. of Aerospace and Mechanical Engineering, 110 Cummington St. Boston, MA 02215; e-mail: dew11@bu.edu
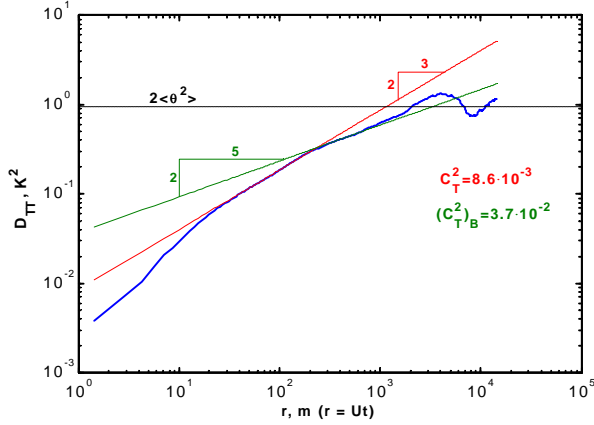
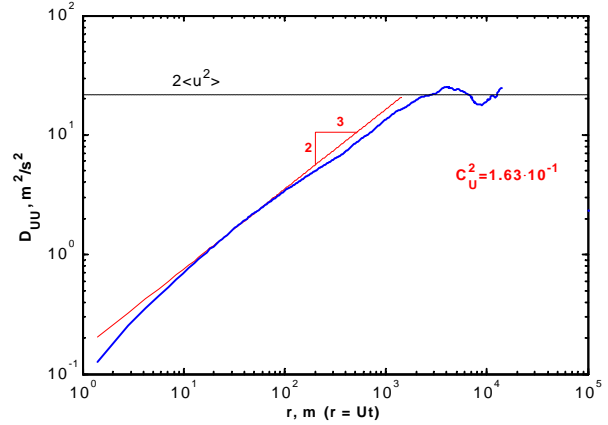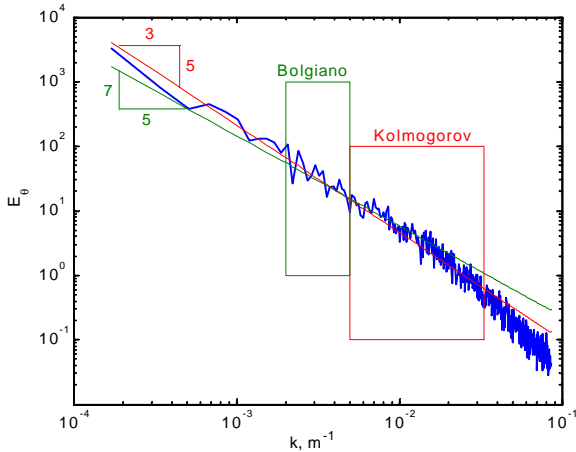Figure 1: Temperature structure function, D_{TT}, for 9.65B km altitude on 990806.

Figure 2: Temperature spectra for 9.65B km altitude on 990806. Boxes denote region of applicability for Bolgiano ($k^{-7/5}$) and Kolmogorov ($k^{-5/3}$) scaling

C_T^2. Note that the drop off below 25 m is consistent with the frequency response roll off of the temperature sensor at frequencies above about 3 hz.

Also evident in Figure 1 is a distinct change in slope at around 200 m, from 2/3 to 2/5, the expected behavior for a buoyancy subrange as predicted by Bolgiano (Monin and Yaglom, 1975). Such a region is generally not identifiable in the spectra. As evidence, consider Figure 2 which shows a temperature spectrum (average of 10 spectra) for the same data used for the structure function in Figure 1, along with the corresponding curve fits corresponding to the Kolmogorov ($k^{-5/3}$) and Bolgiano ($k^{-7/5}$) scaling using the structure constants found from the structure functions. The boxed regions indicate the applicable wavenumber

Figure 3: Velocity structure function, D_{UU}, for 9.65B km altitude on 990806.

ranges for the Kolmogorov and Bolgiano scaling, as determined from the corresponding ranges of r from the structure functions. Two features of this plot are worth noting. First, the spectrum is inherently noisier than the structure function, making it more difficult to identify regions of constant slope. Second, the two lines corresponding to $k^{-5/3}$ and $k^{-7/5}$ are very similar, because the exponents (and hence the slopes on a log-log plot) differ by only 19 percent. Compare this to a difference of almost 67% for the slopes in the structure function plot. It's likely that a region following Bolgiano scaling in the temperature spectra would be interpreted as part of the –5/3 inertial subrange. Thus, the structure function approach facilitates the identification of a Bolgiano subrange, because of the smoothness of the curve and because of the larger relative difference in the slopes compared to the spectra approach.

Figures 3 and 4 show the velocity structure functions (D_{UU}, D_{VV}, and D_{WW}) for the same case as Figure 1. Again, the 2/3 region is clearly seen for D_{UU} over approximately the same range of r seen in D_{TT}. At larger scales, where D_{TT} displayed the 2/5 slope, none of the velocity structure functions exhibit a distinct region characterized by the $r^{6/5}$ scaling that is predicted by the theory of Bolgiano (Monin and Yaglom, 1975, Philips, 1965). Nor is there any region of r^2 slope predicted by Lumley (Lumley, 1965, Philips, 1965).

The structure constants obtained from structure function are compared against those previously found from spectra (Cote, et al., 2000) in Table 1 and Figure 5. The agreement is generally very good, except for the two highest altitudes and the lowest altitude, for which the structure functions generate larger values of both C_T^2 and C_U^2.
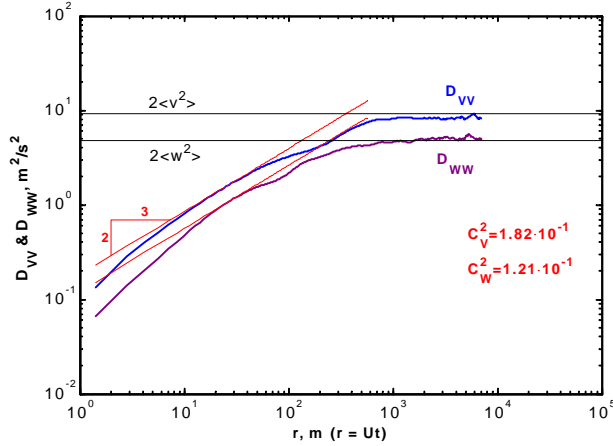
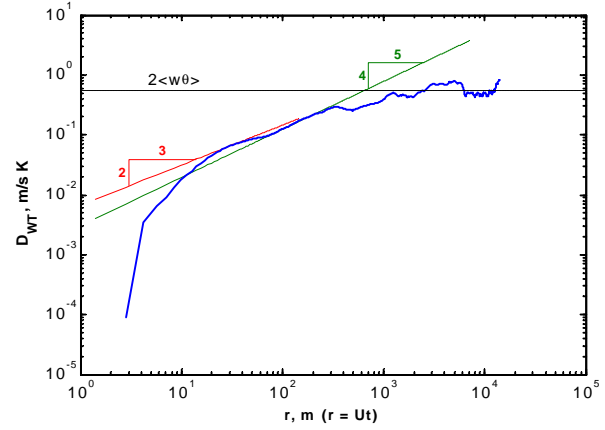Figure 4: Velocity structure function D_{VV} and D_{WW}, for 9.65B km altitude on 990806.

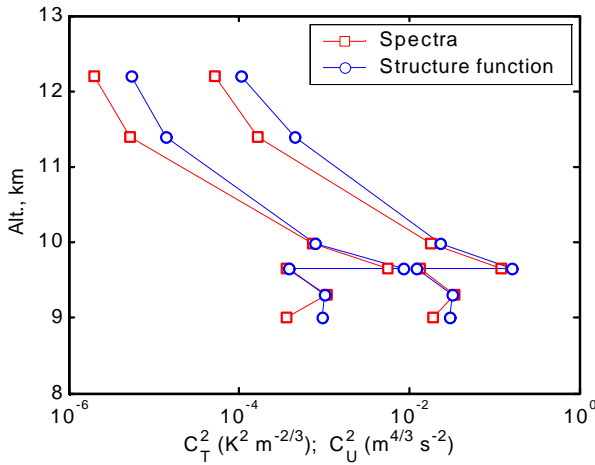Figure 6: Vertical heat flux structure function, D_{WT}, for 9.65B km altitude on 990806

Figure 5: Velocity and temperature structure constants vs. altitude on 980806; comparison of spectra and structure function analysis
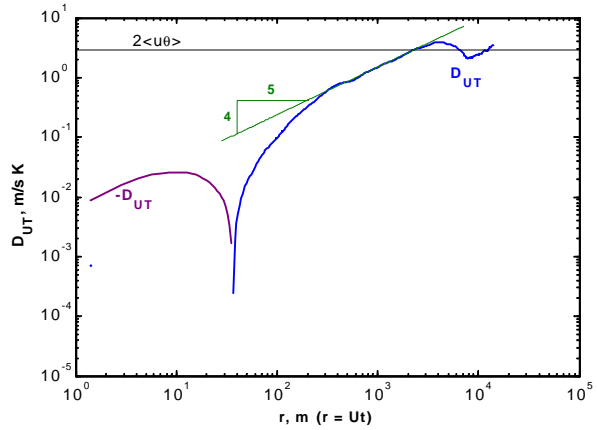

Figure 7: Horizontal heat flux structure function, D_{UT}, for 9.65B km altitude on 990806

For isotropic conditions, $C_W^2 = C_V^2 = 4C_U^2/3$, so that C_W^2/C_U^2 and C_V^2/C_U^2 should equal 1.33. Values of C_V^2/C_U^2, in Table 1, are all approximately 0.93 to 1.1, except for the highest altitude case (also the weakest turbulence case) where the value drops to 0.5. Values of C_W^2/C_U^2, in Table 1, are all less than 1, ranging from 0.21 to 0.59. These results confirm the findings from analysis of the spectra that the turbulence is anisotropic.

Figure 6 shows the heat flux structure function, $D_{WT}(r) = -<[T(t)-T(t+r/U_c)][w(t)-w(t+r/U_c)]>$. Monin and Yaglom (1975) suggest the heat flux should scale as $r^{2/3}$ in the inertial subrange (based on the same scaling parameters that lead to the $r^{2/3}$ behavior in the temperature) and a region obeying this scaling is seen between 20 and 60 m.

Bolgiano scaling of $r^{4/5}$ is also evident, for distances ranging from 70 m up to 200 m. Note that the 2/3 and 4/5 exponents for the inertial and buoyancy subranges are very close, so distinguishing between the two may be difficult. If the heat flux is scaled based on the vertical gradient of the mean potential temperature, then the heat flux should scale as $r^{4/3}$. Such a region is seen in the heat flux structure function, but at separation distances below 30 m, which are affected by the rolloff in the temperature sensor response. It is more likely that such a scaling would be observed at larger scales, which are more affected by mean flow parameters, than at inertial scales, which are presumed to be affected mainly by the energy transferred from large to small scales.
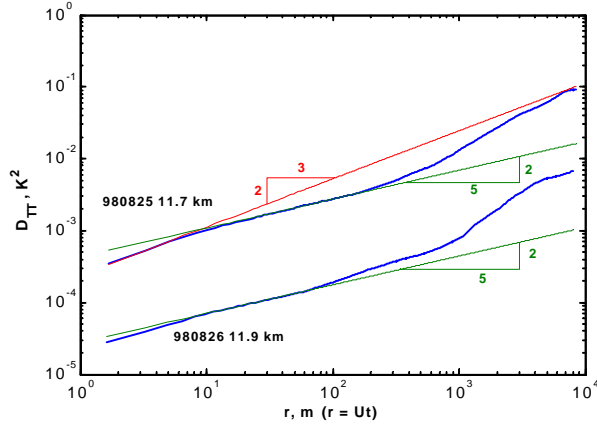
Figure 8: Temperature structure functions, D_{TT}, for 11.7 km on 980825 and 11.9 km on 980826. Note extensive regions of Bolgiano scaling ($r^{2/5}$).

Figure 9: Scaling of buoyancy subrange structure constant, $(C_T^2)_B$. ε and χ are kinetic energy and temperature dissipation.

The structure function for the longitudinal heat flux, seen in Figure 7, exhibits a change in sign at around 30 m, with positive values at larger scales and lower values at smaller scales. This behavior is also observed in the data at 9.0 km, but not in the data at 9.3 km. An extensive region obeying the Bolgiano scaling of $r^{4/5}$ is clearly observed, extending well into the integral scale range.

3. BOLGIANO SCALING

The prevalence of the Bolgiano scaling in the temperature and heat flux structure functions, and its absence from the analysis of spectra, make it worth considering in more detail. Temperature structure functions shown in Figure 8, for the 1998 campaign in Australia, illustrate an interesting feature characteristic of these weaker turbulence cases: the region displaying the 2/5 slope is more dominant than that for the 2/3 slope. For 11.9 km on Aug. 26, no 2/3 slope region is observed within the range of scales analyzed.   For 11.7 km. on Aug. 25, the 2/3 slope region is seen at scales within the frequency regime where sensor lag attenuates the signal. Thus, it is doubtful that this is truly representative of an inertial subrange.

The absence of Kolmogorov scaling has implications for estimation of C_T^2 from temperature measurements obtained at a fixed distance, if that distance falls within the range of scales that obey Bolgiano scaling. Specifically, a different value of C_T^2 will be obtained depending upon the value of r used, $C_T^2 = (C_T^2)_B r^{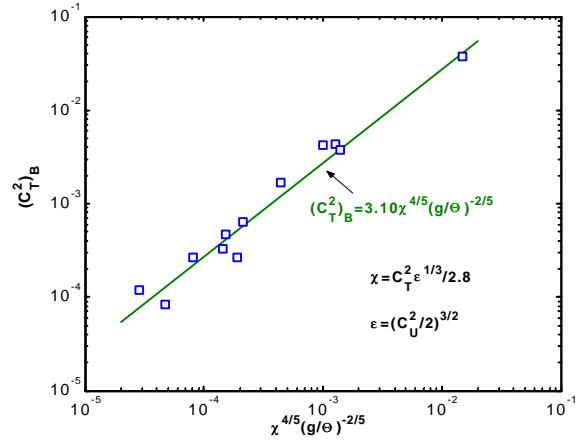-4/15}$ where $(C_T^2)_B = D_{TT} r^{-2/5}$ is a structure constant that defines the buoyancy subrange behavior. For example, the one-meter structure function found from Thermosonde measurements (Jumper and Beland, 2000) would actually represent the buoyancy subrange structure constant, $(C_T^2)_B$.

Komogorov's theory assumes that turbulent kinetic energy is transferred through the inertial subrange unchanged, spanning a region between the production scales and the dissipation scales, resulting in the scaling laws $C_T^2 = C_\theta \chi \varepsilon^{1/3}$ and $C_U^2 = C \varepsilon^{2/3}$ where ε and χ are the kinetic energy and temperature dissipation, and estimates of the constants are $C=2$ and $C_\theta=2.8$. Bolgiano's theory assumes that mean square buoyancy fluctuations are passed through a buoyancy subrange that spans a region between the production scales and the inertial subrange scales, resulting in the scaling laws, $(C_T^2)_B = D_{TT} r^{-2/5} = (C_\theta)_B \chi^{4/5} (g/\Theta)^{-2/5}$ and $(C_U^2)_B = D_{UU} r^{6/5} = (C)_B \chi^{2/5} (g/\Theta)^{4/5}$, where Θ is the potential temperature. The absence of ε in the scaling law for the buoyant subrange arises from the assumption that, for stable stratification, kinetic energy is lost to potential energy due to work against buoyancy, and thus the energy transfer is generally much larger than the dissipation.

The Bolgiano scaling for the temperature was tested through analysis of all data that exhibited a 2/5 slope in D_{TT}, by assuming $\chi = C_T^2 \varepsilon^{1/3}/2.8$ and $\varepsilon = (C_U^2/2)^{3/2}$. $(C_T^2)_B$ was estimated using the same curve-fit approach for finding C_T^2.
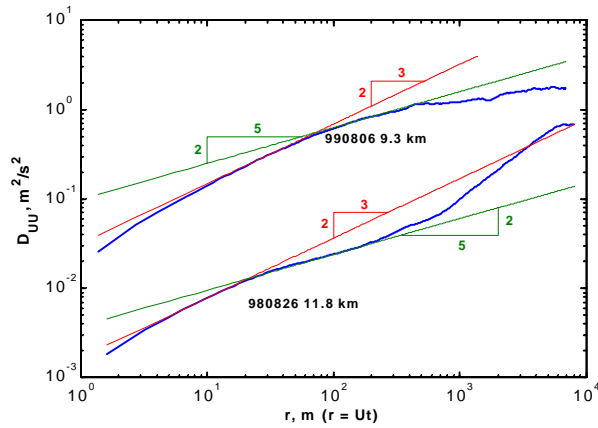
Figure 10: Velocity structure functions, D_{UU}, for 11.8 km on 980826 and 9.3 km on 990806. Note regions of $r^{2/5}$ scaling.

Figure 11: Temperature structure functions, D_{TT}, for 9.4 km and 11.3 km on 980901, illustrating noise at lower separation values.

The relevant data is summarized in Table 2. Note that for cases similar to those shown in Figure 8 (i.e., no Kolmogorov region in D_{TT}) no estimate of χ was possible, so they were not included in the analysis. Figure 9 displays the resulting $(C_T^2)_B$ as a function of $\chi^{4/5}(g/\Theta)^{-2/5}$. A power law curve fit to this data produced an exponent of 1.01, confirming the scaling law, and a value of the constant $(C_\theta)_B$ of 3.1, nearly equal to the corresponding constant in the Kolmogorov scaling C =2.8. The implication of this equality is that the intersection of the two curves, $D_{TT}(r)=C_T^2 r^{2/3}$ and $D_{TT}(r)=(C_T^2)_B r^{2/5}$, is exactly equal to the Oboukhov length scale, $L^*=\varepsilon^{5/4}(g/\Theta)^{3/2}\chi^{-3/4}$. Calculated values of this length scale are also shown in Table 2. Note that for the cases that did not display an $r^{2/3}$ region for D_{TT}, χ was estimated using the curve fit shown in Figure 9. These cases generally involve L^* values on the order of 1 meter or less, i.e., below the smallest scales that could be resolved with the current measurement system and protocol, so the lack of an observable inertial range is to be expected.

One important implication of this result is that, in stronger turbulence, the Oboukhov length is generally on the order of 100 meters or higher, so assumptions of Kolmogorov scaling at smaller scales is generally valid. However, for weaker turbulence, the transition between Kolmogorov and Bolgiano scaling is at much smaller scales, sometimes less than one meter, so care is needed when defining the structure constant from fixed separation distance measurements.

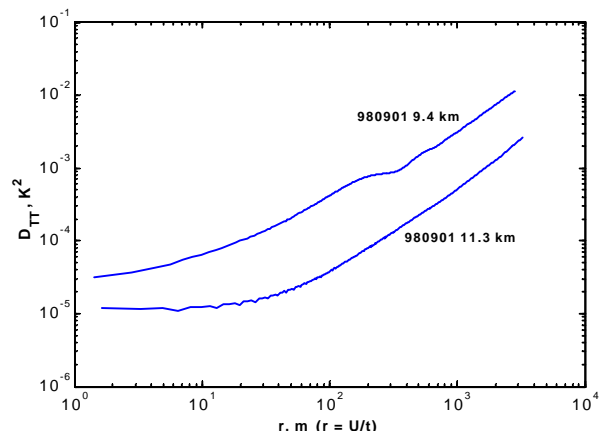Also included in Table 2 is the scaling observed in D_{UU} in the region of separation distances that display Bolgiano scaling in temperature. The predicted $r^{6/5}$ behavior for Bolgiano scaling is not seen in any of these; however, an $r^{2/5}$ behavior is seen in over two thirds of the cases. In fact, the strong turbulence case seen at 9.65B km on 990806 is one of the few cases that do not exhibit this behavior. Several examples of velocity structure functions that do reveal the $r^{2/5}$ behavior are shown in Figure 10. The prevalence of the $r^{2/5}$ scaling in velocity as opposed to the expected $r^{6/5}$ behavior is still an open question at this point.

4. NOISE

The temperature structure function for 11.3 km on 980801, shown in Figure 11, illustrates a characteristic leveling off as r decreases. This represents noise—"white" noise would be expected to exhibit a relatively flat structure function equal to twice the variance of the noise. Thus, the noise floor for these measurements is estimated at approximately 10^{-5} K^2 for D_{TT}, corresponding to a standard deviation of 0.0022 K in the temperature signal. Note that the noise level is observed at different levels for different flights (as high as 10^{-3} K^2 for some of the flights over Wales in 2000), so no single value of noise floor can be stated. However, any value of C_T^2 below about 5×10^{-5} must be treated as suspect, due to the low signal to noise ratio within the expected inertial subrange. In addition, any temperature structure function, like that of the 9.4 km case in Figure 11, displaying a decreasing slope at low values of r (as opposed to the expected increasing slope due to sensor rolloff) should also be suspected of noise contamination.
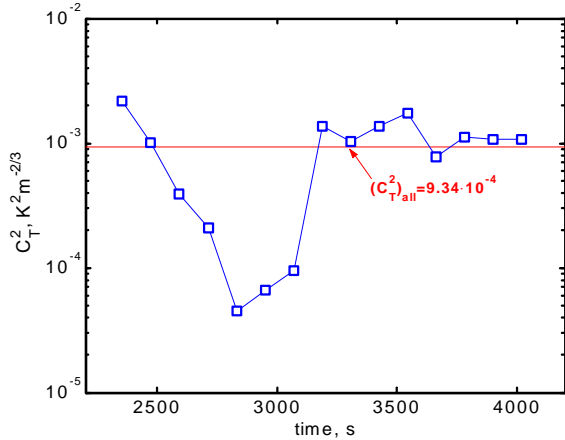
Figure 12: Short-time structure constants as a function of time for 9.0 km on 990806.
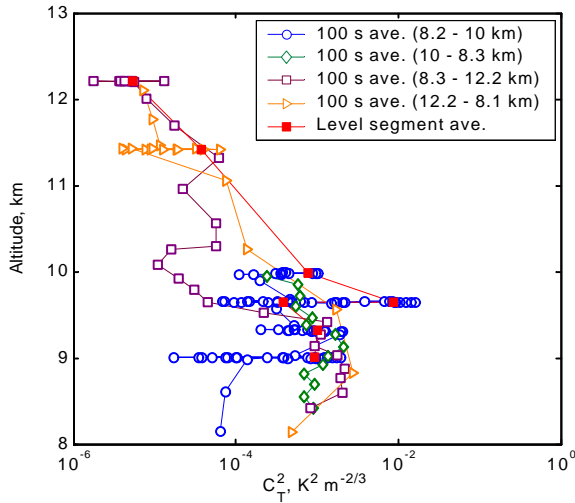

Figure 13: Short-time structure functions for all climb, descent and level flight segments on 990806. Level segment averages are long time averages.

5. SHORT TIME STRUCTURE FUNCTIONS

Most of the level flight segments were 800 to 1,800 seconds long, corresponding to ranges of 60 to 150 km. These long segments were designed to assure sufficient averaging time over the large-scale integral scales of motion. However, it is possible to evaluate C_T^2 for smaller time periods, since the relevant scales for obtaining a meaningful average are associated with scales smaller than the integral scale. Such short time estimates of C_T^2 can be useful because they provide a means of evaluating local C_T^2 and C_n^2 values that may be encountered by an optical beam moving vertically or through a slant path, and because they can be used to compare with

structure constant profiles obtained from Thermosonde balloon flights.

Temperature structure functions were calculated for approximately 100 second intervals, representing 6000 data points. Note that each individual structure function was not evaluated separately to identify a region that obeyed the $r^{2/3}$ power law. Instead, a long-time structure function (like those described above) was found for the entire data record, and that was used to identify a range of r that displayed the $r^{2/3}$ behavior. For all of the short-time segments spanning that data record, C_T^2 was estimated by averaging the value of $D_{TT}r^{-2/3}$ within the chosen range of r. For some segments, this was just an estimate, particularly in segments associated with very low C_T^2, because of the noise floor.

The short time values of C_T^2 for 9.0 km on 990806, shown in Figure 12, exhibit a significant variation over the 1,700 second level flight segment, spanning close to two orders of magnitude. In particular, a low turbulence, quiet period is observed during the mid portion of the segment. Although this represents an extreme case, most of the other segments analyzed displayed variations that spanned at least an order of magnitude. Thus, a single long-time measurement of C_T^2 does not necessarily reflect the local behavior that may be encountered by a beam propagating lateral to the layer. However, long-time averages are still required for overall statistics used for evaluating variances, correlations and turbulent budgets.

Short time values of C_T^2 were found for all of the flight segments on 990806, including climb and descent portions. These are shown as a function of altitude in Figure 13. The chronology of the flight segments follows the order shown in the legend: (1) climb to 10 km with level flight segments at 9.0, 9.3, 9.65 and 9.98 km; (2) descend to 8.3 km; (3) climb to 12.2 km with level flight segment at 12.2 km; and (4) descend from 12.2 km, with a level flight segment at 11.4 km. It is interesting to note that the strong turbulence seen during the second half of the level segment at 9.65 km (the 9.65 B case discussed above) is not observed during the three subsequent passes through that altitude during segments 2, 3 and 4. In particular, the level of turbulence seen is particularly weak during the segment 3 ascent at both 9.65 and 9.98 km. In contrast, at lower altitudes, the turbulence during the subsequent descent and climb portions tend to be at the stronger side of the range measured during the level flight segments.
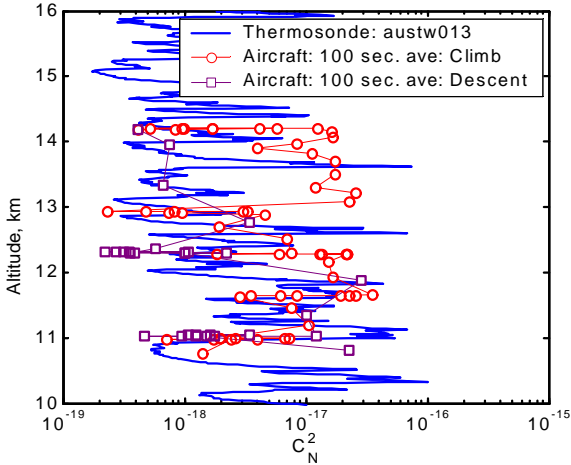
Figure 14: Comparison of short-time refractive structure constant, C_N^2, from aircraft and Thermosonde measurements for 980825.
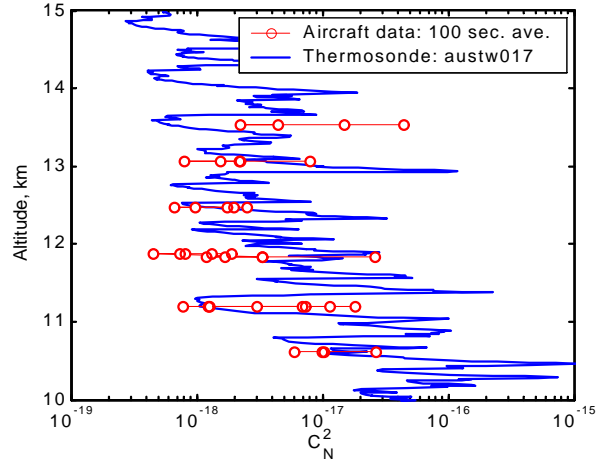

Figure 15: Comparison of short-time refractive structure constant, C_N^2, from aircraft and Thermosonde measurements for 980826.

It should be mentioned that the passes through a given altitude do not correspond to sampling at the same location, and may represent locations separated by hundreds of kilometers. Analysis of the longitude and latitude provided by the aircraft's GPS sensor might provide additional information regarding the structure of the turbulence. In addition, it is suggested that subsequent aircraft campaigns adopt flight plans that could return to the same location so that changes in time may be determined as well.

For two days during the 1998 Australia campaign, 980825 and 980826, a similar short-time C_T^2 analysis was extended to calculations of C_n^2, refractive index structure function, using the formula $C_n^2 = (79 \times 10^{-8} \, P/T^2)^2 \, C_T^2$. The results are compared with balloon Thermosonde data obtained at the same time as the flights. The Thermosonde measures temperatures from two cold-wire probes attached to the ends of a 1 meter boom, and determines a moving rms average of the difference. Assuming Kolmogorov scaling, the square of the rms signal is the structure constant C_T^2, with data averaged every 1.2 seconds.

As seen in Figure 14 and Figure 15, the variations in the short time structure function from the aircraft measurements at a given altitude span approximately the same range as the variations in the Thermosonde data. This provides some evidence that the two techniques are providing similar measurements of refractive turbulence, since the wide variations seen from the aircraft data at a given altitude generally encompass the short-time measurements seen from the Thermosonde. Beyond that, detailed comparisons

of the shapes of the curves are difficult, since data were not obtained at the same time and because of the much shorter averaging time for the Thermosonde. It is interesting to note that during the aircraft climb from 13 to 14 km on 980825 (Figure 14), the turbulence was strong, consistent with the Thermosonde peak at about 13.5 km, while the descent segment sampled much less turbulent air, consistent with the levels of C_n^2 seen above and below the peak.

The large variations in C_n^2 at a given altitude may shed doubt on one of the approaches used for modeling the horizontal structure of turbulent layers for computing optical effects. The so-called "onion-skin model" assumes that C_n^2 measurements from the Thermosonde at any altitude are uniform over the entire horizontal extent of the problem considered. It is clear from the aircraft data that a horizontal layer features large variations in C_n^2. Even the use of a long-time average layer value might be questionable, since the integration is weighted differently over the path depending upon the type of beam.

6. INTEGRAL LENGTH SCALES AND HOMOGENEITY

The variations seen in structure constant at a given altitude may be due to inhomegeneity in the turbulence field or, since they represent averages over scales smaller than the integral scale, may simply be due to the natural intermittency, or bursting nature, of the turbulence. An integral length scale, $L_\theta = (\theta^2/C_T^2)^{3/2}$, can be calculated for each of the short time segments to explore this issue. Note that θ^2 would be the short-time
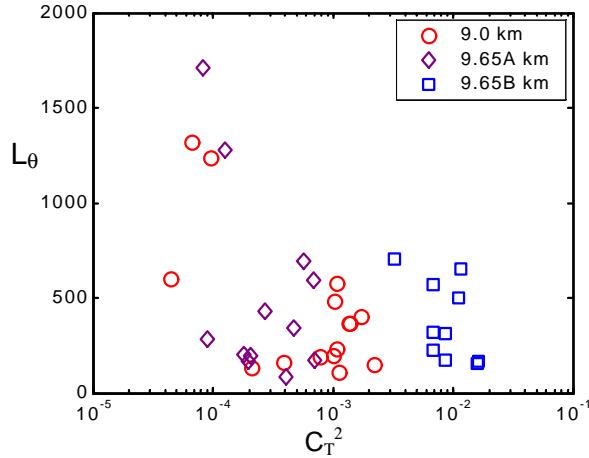
Figure 16:   Short-time integral length scale, $L_\theta = (\theta^2/C_T^2)^{3/2}$, as a function of short-time C_T^2 for 9.0, 9.65A, 9.65B km on 990806
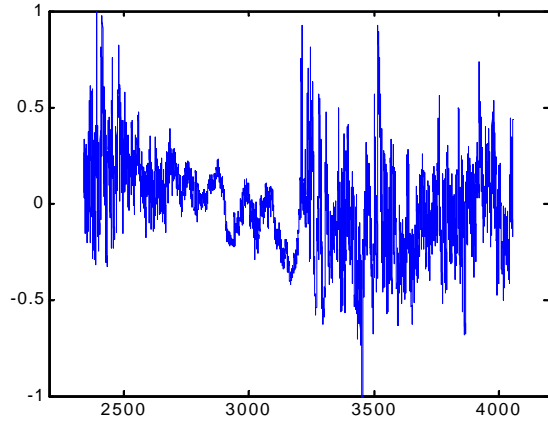

Figure 17:   Raw temperature time series for 9.0 km on 980806. Note low turbulence period around 3,000 seconds and wave-like motions.

Figure 18:   Temperature time series for 9.0 km on 980806, filtered using 1001 point moving average. Note smaller variations during low turbulence period.

variance of the temperature signal.   Figure 16 shows this length scale as a function of the short time structure function, for three of the level flight segments for 990806, including the 9.0 km case shown in Figure 12. Most of the values fall within a range from 100 meters to 600 meters, with the exception of four segments-- two at 9.0 km and two at 9.65A km. All four are associated with low values of C_T^2, representing relatively quiet periods, suggesting possible non-homogeneity in the layer. However, another explanation is possible.

The temperature signal for the 9.0 km case, Figure 17, clearly displays the low turbulence region, centered around 3,000 seconds, which accounts for the large drop in C_T^2 seen in Figure 12.   However, note that during this period, the temperature displays a definite wave-like pattern. This wave-like pattern is present in all of the 990806 data, but is most easily seen in the 9.0 km data during the low-turbulence segments.   The large length scales seen for these lower turbulence periods may be due to high short time variances associated with the larger-scale wave-like motions. To explore this, the temperature was detrended using a 1001-point moving average. The resulting signal, seen in Figure 18, is similar to a low-pass filtered signal with a cutoff frequency of 0.03 Hz, corresponding to a length scale of approximately 2.8 km.   Note that the filtering does not affect the values of C_T^2, since the length scales associated with the inertial subrange (less than 100 m) are much smaller than the filtering length scale.

If the filtered signal is used to calculate the short-time variances and the integral scales, the large values of L_θ associated with weaker turbulent periods now fall within the same range as the rest of the data, Figure 19.   Although the values for L_θ still vary over a range from 20 to 200 m, this variation is likely within the accuracy of the measurements. Thus, it can be presumed that the layers are mostly homogeneous, and that the variations in short-time C_T^2 are associated with variations of the turbulence levels within the layer.

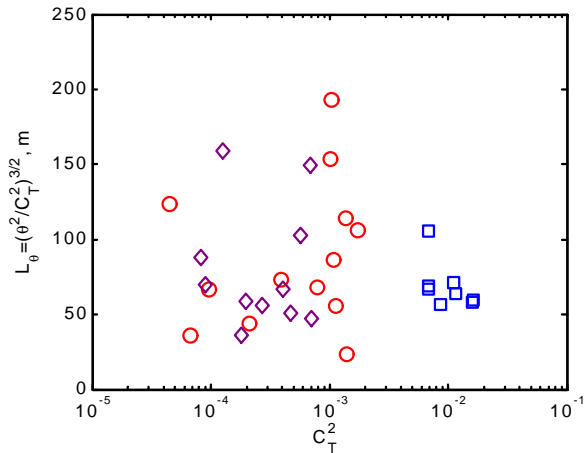Figure 19: Short-time integral length scale, $(\theta^2/C_T^2)^{3/2}$, calculated using filtered temperature signal, as a function of short-time C_T^2 for 9.0, 9.65A, 9.65B km on 990806

As a final check on this conclusion, the long-time-average integral length scales for all of the 990806 levels were found using both raw and detrended temperature data. As seen in Table 3, the low turbulence observed at 11.4 and 12.5 km yield excessively large integral scales (100's of km), and even the 9.98 km case exhibited a length scale much larger than those at the lower altitudes. When filtered data is used, the lengths scales for all layers fall within a range from 45 to 106 meters, with an average value of 78 meters and a standard deviation of 19 meters. Table 3 also shows length scales calculated based on the buoyancy subrange structure constants, $L_{\theta,B}=[\theta^2/(C_T^2)_B]^{5/2}$. These values fall within an even smaller range, from 29 meters to 43 meters, with an average value of 35 meters and a standard deviation of only 6 meters. These results indicate that the turbulence seen at all layers is fairly homogeneous, a fact that is obscured if detrending is not used to filter large-scale motions that are not necessarily representative of the turbulent structure.

The detrending of atmospheric turbulence data is a critical issue, and will not be discussed in detail here. Filtering of large-scale variations from the turbulence signals (on the order of km), using moving-average deterending should not effect the calculations of C_T^2. However, filtering is important when evaluating variances and correlations (like the heat flux) for use in budgets and length scale calculations.

7. CONCLUSIONS

This work has demonstrated that determination of structure constants is more easily accomplished through analysis of structure functions than from spectra, because the structure functions are less noisy, facilitating the identification and fitting of constant slope regions on a log-log plot. In addition, it is easier to identify small changes in slope associated with transitions from Kolmogorov scaling to Bolgiano scaling.

It should be noted that structure functions do not provide the same information as spectra. The spectrum represents energy contained at various *independent* wavenumbers. The structure function at a given separation distance is actually a weighted average of the energy over the entire wavenumber range. Nonetheless, each has its use, and the structure function seems well suited for determination of structure constants.

For much of the data from the 1998 and 1999 flights over Australia, the temperature structure functions exhibited a distinct change in slope from 2/3 to 2/5, the expected behavior for a buoyancy subrange as predicted by Bolgiano. In some cases of weaker turbulence, the region of 2/5 slope was more dominant than the inertial subrange, extending over a greater range of scales. The buoyancy subrange scaling that leads to the $r^{2/5}$ scaling predicts that a temperature structure function for such a region would be given by $(C_T^2)_B=D_{TT}/r^{2/5} =C\chi^{4/5}(g/\Theta)^{-2/5}$. Analysis of data that exhibited a 2/5 slope indicated that this correlation was well obeyed over several orders of magnitude, and showed that the constant C was nearly the same as the corresponding constant for Kolmogorov scaling. The velocity structure function did not exhibit the expected $r^{6/5}$ predicted for Bolgiano scaling, but instead featured an $r^{2/5}$ scaling for the majority of the cases that displayed a $r^{2/5}$ scaling for temperature.

Short-time structure constants (100 second averages) were used to study the horizontal structure of the turbulent layers and to compare aircraft results with Thermosonde measurements. The horizontal structures were characterized by large variations in C_T^2-- as much as two orders of magnitude. These results cast doubt on the use of the simplified "onion-skin model" which assumes that Thermosonde measurements of C_T^2 at a given altitude are uniform over the horizontal extent of propagation. Calculations of short-time integral scales revealed that the layers were mostly homogeneous and that the variations in the short-time C_T^2 tracked the variations in short time variances, as long as the contributions to the

variances from large-scale wave-like motions were filtered out of the signal.

Comparisons of short-time C_n^2 values with Thermosonde measurements revealed reasonable agreement, within the constraints posed by the differences in the techniques. In particular, the variations in C_n^2 at a given altitude, were approximately the same as the variations observed in the Thermosonde measurements as it ascended vertically through a high turbulence layer.

Although information on structure constants can be obtained from short-time averages, it is still recommended that long data sampling periods be used for characterizing horizontal layers for two reasons: first, the long-time averages are still needed for variances and heat flux calculations required for turbulent budgets and second, the variations in C_T^2 through a layer provide insight into the extent of conditions that might be encountered.

8. ACKNOWLEDGEMENTS

9. REFERENCES

Cote, O. R., J. M Hacker, T. L. Crawford, and R. J. Dobosy, 2000, "Clear air turbulence and refractive turbulence in the upper troposphere and lower stratosphere," *Ninth Conf. on Aviation, Range, and Aerospace Meteorol.*

Jumper, G. Y., and R. R. Beland, 2000, "Progress in Understanding and Modeling of Atmospheric Optical Turbulence," AIAA-2000-2355.

Lumley, J. L., 1965, "Theoretical Aspects of Research on Turbulence in Stratified Flows," Proceedings of the International Colloquium on Atmospheric Turbulence and Radio Wave Propagation, Moscow, June 15-22, pp. 105-110.

Monin, A. S. and A. M. Yaglom, 1975, *Statistical Fluid Mechanics*, MIT Press, Cambridge, MA.

Philips, O. M., 1965, "On the Bolgiano and Lumley-Shur Theories of the Buoyancy Subrange," Proceedings of the International Colloquium on Atmospheric Turbulence and Radio Wave Propagation, Moscow, June 15-22, pp. 121-128.

Table 1: Comparison of structure constants obtained from analysis of structure functions (SF) with those obtained from analysis of spectra (Sp) (Cote, et al., 2000).

Alt., km		9.00	9.32	9.65A	9.65B	9.99	11.4	12.2
C_T^2	SF	$9.40\ 10^{-4}$	$1.02\ 10^{-3}$	$3.89\ 10^{-4}$	$8.60\ 10^{-3}$	$7.82\ 10^{-4}$	$1.41\ 10^{-5}$	$5.48\ 10^{-6}$
	Sp	$3.67\ 10^{-4}$	$1.08\ 10^{-3}$	$3.66\ 10^{-4}$	$5.57\ 10^{-3}$	$7.27\ 10^{-4}$	$5.26\ 10^{-6}$	$2.00\ 10^{-6}$
C_U^2	SF	$3.02\ 10^{-2}$	$3.19\ 10^{-2}$	$1.23\ 10^{-2}$	$1.63\ 10^{-1}$	$2.29\ 10^{-2}$	$4.59\ 10^{-4}$	$1.07\ 10^{-4}$
	Sp	$1.90\ 10^{-2}$	$3.42\ 10^{-2}$	$1.34\ 10^{-2}$	$1.20\ 10^{-1}$	$1.79\ 10^{-2}$	$1.68\ 10^{-4}$	$5.30\ 10^{-5}$
C_V^2,	SF	$3.43\ 10^{-2}$	$3.31\ 10^{-2}$	$1.41\ 10^{-2}$	$1.82\ 10^{-1}$	$2.60\ 10^{-2}$	$4.26\ 10^{-4}$	$5.37\ 10^{-5}$
	Sp	$2.66\ 10^{-2}$	$3.43\ 10^{-2}$	$1.48\ 10^{-2}$	$1.31\ 10^{-1}$	$2.30\ 10^{-2}$	$5.20\ 10^{-4}$	$5.33\ 10^{-5}$
C_W^2	SF	$1.78\ 10^{-2}$	$1.84\ 10^{-2}$	$6.40\ 10^{-3}$	$1.21\ 10^{-1}$	$1.12\ 10^{-2}$	$1.15\ 10^{-4}$	$2.30\ 10^{-5}$
	Sp	$1.16\ 10^{-2}$	$1.80\ 10^{-2}$	$5.75\ 10^{-3}$	$1.00\ 10^{-1}$	$1.03\ 10^{-2}$	$3.94\ 10^{-5}$	$2.05\ 10^{-5}$
C_U^2/C_T^2	SF	32	31	32	19	29	33	20
	Sp	51.8	31.5	36.6	21.5	24.6	31.9	26
C_V^2/C_U^2	SF	1.1	1.0	1.1	1.1	1.1	0.93	0.5
	Sp	1.4	1	1.1	1.1	1.3	1.26	1
C_W^2/C_U^2	SF	0.59	0.58	0.52	0.74	0.49	0.25	0.21
	Sp	0.61	0.52	0.43	0.83	0.58	0.23	0.38
C_W^2/C_T^2	SF	19	18	16	14	14	8.2	4.2
	Sp	32	17	16	18	14	7.5	10

Table 2: Data used for analysis of Bolgiano scaling analysis.

Alt km	$(C_T^2)_B$ $K^2 m^{-2/5}$	C_T^2 $K^2 m^{-2/3}$	χ $K^2 s^{-1}$	C_U^2 $m^{4/3} s^{-1}$	ε $m^2 s^{-3}$	Θ K	L^* m	$r^{2/5} D_{UU}$ scaling
990806 Australia								
9.00	$4.36\ 10^{-3}$	$9.40\ 10^{-4}$	$4.13\ 10^{-5}$	$3.02\ 10^{-2}$	$1.86\ 10^{-3}$	336.0	150	Y
9.30	$3.75\ 10^{-3}$	$1.02\ 10^{-3}$	$4.60\ 10^{-5}$	$3.19\ 10^{-2}$	$2.01\ 10^{-3}$	338.2	155	Y
9.65B	$3.70\ 10^{-3}$	$8.60\ 10^{-3}$	$8.77\ 10^{-4}$	$1.63\ 10^{-1}$	$2.33\ 10^{-2}$	341.0	366	N
9.65A	$1.69\ 10^{-3}$	$3.89\ 10^{-4}$	$1.09\ 10^{-5}$	$1.23\ 10^{-2}$	$4.82\ 10^{-4}$	341.0	77	Y
9.98	$4.20\ 10^{-3}$	$7.82\ 10^{-4}$	$2.99\ 10^{-5}$	$2.29\ 10^{-2}$	$1.23\ 10^{-3}$	342.8	117	Y
11.4	$4.56\ 10^{-5}$	*	*	$4.59\ 10^{-4}$	$3.48\ 10^{-6}$	357.0	2.42	Y
980825 Australia								
11.7	$4.35\ 10^{-4}$	*	*	$4.94\ 10^{-4}$	$3.88\ 10^{-6}$	354.3	0.33	Y
12.3	$4.19\ 10^{-4}$	*	*	$3.20\ 10^{-4}$	$2.02\ 10^{-6}$	360.7	0.16	N
12.9	$5.09\ 10^{-5}$	*	*	$5.59\ 10^{-4}$	$4.67\ 10^{-6}$	369.6	3.36	Y
980825 Australia (“Strong” Turbulence Events) **								
11.0	$3.25\ 10^{-4}$	$1.08\ 10^{-4}$	$2.66\ 10^{-6}$	$9.44\ 10^{-3}$	$3.24\ 10^{-4}$	347.6	140	Y
11.7	$6.68\ 10^{-4}$	*	*	$9.39\ 10^{-4}$	$1.02\ 10^{-5}$	354.3	0.69	Y
12.3	$5.52\ 10^{-4}$	*	*	$1.10\ 10^{-3}$	$1.29\ 10^{-5}$	360.5	1.14	Y
14.2	$2.64\ 10^{-4}$	$1.20\ 10^{-4}$	$3.53\ 10^{-6}$	$1.37\ 10^{-2}$	$5.67\ 10^{-4}$	386.5	266	N
980826 Australia								
10.6	$4.66\ 10^{-4}$	$1.10\ 10^{-4}$	$2.92\ 10^{-6}$	$1.11\ 10^{-2}$	$4.13\ 10^{-4}$	332.5	165	Y
11.8	$2.80\ 10^{-5}$	*	*	$1.70\ 10^{-3}$	$2.48\ 10^{-5}$	344.5	38.0	Y
13.5	$8.32\ 10^{-5}$	$3.27\ 10^{-5}$	$6.60\ 10^{-7}$	$6.40\ 10^{-3}$	$1.81\ 10^{-4}$	351.9	195	Y
980901 Australia								
6.9	$1.20\ 10^{-4}$	$4.20\ 10^{-5}$	$3.64\ 10^{-7}$	$1.18\ 10^{-3}$	$1.43\ 10^{-5}$	324.5	11.3	Y
14.7	$5.51\ 10^{-5}$	*	*	$1.35\ 10^{-4}$	$5.55\ 10^{-7}$	379.9	0.21	Y
980903 Australia								
12.6	$2.73\ 10^{-5}$	*	*	$1.10\ 10^{-3}$	$1.29\ 10^{-5}$	355.5	18.7	N
13.2	$2.68\ 10^{-4}$	$8.34\ 10^{-5}$	$1.27\ 10^{-6}$	$3.64\ 10^{-3}$	$7.76\ 10^{-5}$	360.4	43.0	N
990213 Japan								
7.9	$6.38\ 10^{-4}$	$2.03\ 10^{-4}$	$4.53\ 10^{-6}$	$7.80\ 10^{-3}$	$2.44\ 10^{-4}$	321.0	58.1	N

Notes: *   No $r^{2/3}$ region observed in D_{TT}. χ estimated for calculation of L^*.
         ** Analysis of short segment of data that showed strong turbulence.

Table 3: Integral length scales for 980806 data.

Altitude km	L_θ, raw km	L_θ, detrended, m *	$(L_\theta)_B$ detrended m *
9.0	0.43	75	29
9.3	0.60	66	41
9.65B	0.40	86	43
9.65A	1.19	76	35
9.98	0.51	106	35
11.4	131	45	30
12.6	286	90	NA

Notes: $L_\theta = (\theta^2/C_T^2)^{3/2}$ $L_{\theta,B} = [\theta^2/(C_T^2)_B]^{5/2}$

  * Calculated using variance found from temperature signal detrended using 1001 point moving average.